International Journal of Solids and Structures 50 (2013) 1869–1878

Contents lists available at SciVerse ScienceDirect

International Journal of Solids and Structures

journal homepage: www.elsevier.com/locate/ijsolstr

Determination of the intrinsic behavior of polymers using digital image correlation combined with video-monitored testing

X. Poulain [a], L.W. Kohlman [b], W. Binienda [b], G.D. Roberts [c], R.K. Goldberg [c], A.A. Benzerga [a,d,*]

[a] Department of Aerospace Engineering, Texas A&M University, College Station, TX 77843, USA
[b] The University of Akron, Akron, OH 44325, USA
[c] NASA Glenn Research Center, Cleveland, OH 44135, USA
[d] Materials Science and Engineering Program, Texas A&M University College Station, TX 77843, USA

ARTICLE INFO

Article history:
Received 14 October 2012
Received in revised form 14 December 2012
Available online 16 February 2013

Keywords:
Plastic instability
Large strain behavior
True stress–strain measurement
Tension–compression asymmetry

ABSTRACT

Three methods for the determination of the large-strain behavior of ductile polymers are compared in both tension and compression. Each method relies on some (non-contact) measurement of the strain and some approximations in the calculation of stress. The strain measurement techniques include digital image correlation (DIC) and two techniques of video-based extensometry: marker tracking and area variation monitoring. Since the specimens are inevitably subject to structural plastic instabilities (necking in tension, barreling in compression) the strain and stress states are no longer uniform in the gauge section after the peak load. Under such circumstances, it is demonstrated that the three experimental methods can lead to significant differences. It is inferred from the comparative analysis that the method based on vertical marker tracking is not reliable. Validated by DIC, video-based area variation is shown to be a simple alternative way to obtain an excellent estimate of the intrinsic true stress–strain behavior of the polymer.

1. Introduction

Experimental characterization of the large-strain constitutive behavior of materials is a challenging task. The principal difficulty resides in accounting for specimen-level geometry changes that accompany large deformations. The task is further complicated by the fact that the deformation and stress fields quickly become nonuniform within the specimen. This nonuniformity manifests itself through necking in tension and barreling in compression. Both necking and barreling are plastic instabilities. As such, they are not dependent on the intrinsic material behavior only, but also on the specimen geometry. Therefore, a key step in data interpretation and analysis is to decouple, if at all possible, the structural effects from the intrinsic behavior.

Glassy polymers, for instance, exhibit some viscoelastic deformation, large inelastic strains with small-strain softening and large-strain rehardening. The post-yield softening is dependent upon the thermomechanical history (van Melick et al., 2003a) and is believed to be associated with free-volume rearrangement (Hasan et al., 1993) whereas the rehardening at large strains depends on network density (van Melick et al., 2003b) and results from an induced anisotropy due to molecular chain reorientation (Haward and Thackray, 1968). Because of this peculiar behavior, initially smooth bars of glassy polymers are subject to the propagation of necks along their axis, when strained in tension (Buisson and Ravi-Chandar, 1990; Parsons et al., 2004). Shear bands may trigger or accompany neck propagation and other similar complex patterns of localized deformation may form under compression (Bowden and Jukes, 1968). What is of particular significance is that conventional methods cannot be used to infer the intrinsic material behavior from the mechanical response of a specimen in the presence of plastic instabilities or macroscopic localization. For example, the post-peak strain softening observed in nominal stress–strain data is not representative of the material behavior, e.g. see Ravi-Chandar and Ma, 2000. More generally, while the qualitative features of the uniaxial behavior are rather well known, it remains that determining the quantitative response depends on the way in which the structural effects are decoupled from the polymer's intrinsic behavior.

To address these challenges, several approaches have been followed in the literature. One approach is to design the experiment so as to delay the onset of localization and extract the material behavior from specimens showing macroscopically homogeneous deformation. Thus, platen lubrication in uniaxial compression experiments has been shown to delay significantly barrel formation (Boyce and Arruda, 1990; Arruda et al., 1995; Liang and Liechti, 1996) but is unlikely to suppress it completely (Ravi-Chandar and Ma, 2000; Benzerga et al., 2004; Wu and Buckley, 2004). Other

* Corresponding author at: Materials Science and Engineering Program, Texas A&M University College Station, TX 77843, USA.
E-mail address: benzerga@tamu.edu (A.A. Benzerga).

0020-7683/$ - see front matter © 2013 Elsevier Ltd. All rights reserved.
http://dx.doi.org/10.1016/j.ijsolstr.2013.01.041

examples include custom-designed shear specimens (G'Sell and Gopez, 1981; Santore et al., 1991; Liang and Liechti, 1996) and confined compression (Ma and Ravi-Chandar, 2000). While promising, this approach has had limited success. In shear specimens, exploitable ranges of shear strain remain small, because of premature fracture in sheet specimens (Ravi-Chandar and Ma, 2000) or strain localization near the specimen corners in rail-shear specimens (G'Sell and Gopez, 1981; Santore et al., 1991). While larger strain levels can be reached in confined compression, they remain smaller than about 0.15. In addition, the stress state is multiaxial which complicates the analysis of tests. Another approach is to use strain gauges (Liang and Liechti, 1996; Goldberg et al., 2005). This method is obviously limited by the maximum range of the strain gauge. In addition, it has been shown that strain gauges induce local stress concentrations, which promote premature fracture (Goldberg et al., 2005); for example, tensile strains were limited to less than 0.1 in ductile polymers capable of much greater straining (Liang and Liechti, 1996).

Yet another approach is to record full-field measurements of mechanical fields in deformed specimens. Particularly useful for heterogeneous materials, this approach potentially allows the determination of the intrinsic behavior *locally*, thus circumventing the complications due to specimen-level geometric instabilities. Real-time full-field strain determination is typically made using deposited grid patterns (Buisson and Ravi-Chandar, 1990), geometric Moiré techniques (Liang and Liechti, 1996; Shield and Kim, 1991) and, in recent years, using digital image correlation (DIC) (Hild and Roux, 2006; Laraba-Abbes et al., 2003; Parsons et al., 2004; Grytten et al., 2009; Fang et al., 2009; Littell et al., 2008). More difficult is the determination of stress fields. Extensions of photoelastic methods have been proposed and used (Buisson and Ravi-Chandar, 1990; Liang and Liechti, 1996), but remain difficult to generalize. Thus, when full-field strain data is available there often remains the question of stress determination. When the wavelength of nonuniform strain fields is larger than the characteristic grid/facet size, it is reasonable to back-estimate the local stress assuming homogeneous deformation at the scale of grid element. However, some difficulties having both fundamental and practical origins remain. For instance, the location of the maximum plastic strain is generally not fixed. In addition, unloading may occur locally due to instabilities sweeping by the location of interest. Also, the calculated stress is based on the *net* force acting on a much greater area. Finally, the strain measurements are limited to the surface.

In another set of studies, variants of Video-based Surface Extensometry (VSE) have been developed (G'Sell et al., 2002; Gloaguen and Lefebvre, 2001; Mohanraj et al., 2006). Axial and/or transverse displacements of markers printed prior to the test are tracked to determine local strains. In all of these, the stress is calculated assuming homogeneous deformation of the specimen at some level.

An alternative method that has been used in tension experiments consists of measuring the instantaneous minimum diameter using either a diametral transducer (G'Sell and Jonas, 1979) or a video-based radial extensometer (VRE) (G'Sell et al., 1992; Mohanraj et al., 2006). Effective conjugate measures of strain and stress can thus be obtained. This method has extensively been used by G'Sell and co-workers and bears conceptual affinity with methods used for ductile metals, e.g. (Beremin, 1981; Benzerga et al., 2004). In the case of ductile polymers, the superiority of non-contact video-based extensometry is without doubt. For example, besides the risk of slippage along the neck, diametral transducers may cause premature failure, an effect which is somewhat similar to that of strain gauges. To our knowledge, methods based on video extensometry have not yet been validated against full-field strain measurements.

In this work, real-time DIC full-field strain measurements are used to critically assess how effective video extensometry is at obtaining the intrinsic behavior of a ductile epoxy polymer up to large strains. Both techniques of video extensometry are probed: VSE based on markers and VRE based on diameter measurement. Cylindrical specimens were used for both tension and compression, building on previous work of Littell et al. (2008). The sensitivity of material properties, such as hardness, ductility and post-yield drop, to the type of approximate true stress and strain measures is critically discussed.

2. Methods

2.1. Material

The material used in this study is a commercial untoughened thermosetting epoxy E-862 manufactured in plate form by North Coast Composites using a pressurized resin transfer molding process. The polymer is formed from the reaction of epoxide resin EPON resin 862 (Diglycidyl ether of bisphenol F -DGEBF-) with the aromatic amine curing agent Epikure W which is mainly composed of diethyltoluenediamine (DETDA). The degree of polymerization of EPON resin, which results from the reaction of an epoxide and bisphenol F, is controlled by temperature. This curing reaction is carried out at 176 °C (350 °F). The addition of the curing agent DETDA creates a highly cross-linked network (Tack and Ford, 2008). When the appropriate curing agents are used to cross-link Epon 862, higher electrical, adhesive, chemical and mechanical properties are reached. Also, because of its wide availability, low viscosity and high glass transition temperature (T_g=133 °C (Gilat et al., 2007)), this resin has recently been selected as potential candidate for use in impact resistant materials.

2.2. Testing procedure

All mechanical testing was conducted under quasi-static conditions on a tabletop MTS model 858 servo-hydraulic machine, as previously reported (Littell et al., 2008). Here, a description of the test procedure is reviewed for completeness. Round smooth bars were cut out of a 0.25" thick plate. The use of a cylindrical shape eliminates corners that are often the site of defects and associated stress concentrations in specimens with rectangular cross-section which have been cut from plates. Another benefit of using the precision machined cylindrical geometry is that variation in cross-sectional area is minimized without using the laborious polishing procedures that would be needed for specimens with rectangular cross-section. The cylindrical geometry also allows for a better assessment of induced anisotropy during plastic deformation. In thin sheet specimens, through-thickness necking can lead to a "structural" anisotropy.

Specimen geometry and dimensions were derived from those of an ASTM standard tensile specimen (ASTM, 2008), and are given in Fig. 1. The bars were smaller than standard specimens because of the plate thickness constraint. The small specimen size also leads to a lower probability of internal (processing-related) voids in the gauge section. A smooth surface finish was achieved in the gauge section using a computer numerical controlled (CNC) lathe process. The same specimens were used for compression testing. In addition to being convenient, the common geometry increases the propensity to strain localization under compression. This constitutes a further test for the proposed methodology, which aims at extracting the intrinsic polymer behavior in the presence of structural instabilities.

The specimens were tested in tension and compression at room temperature and at various values of the nominal strain rate (crosshead speed/initial gauge length). At least three, and up to seven realizations of the same test condition were carried out. Other

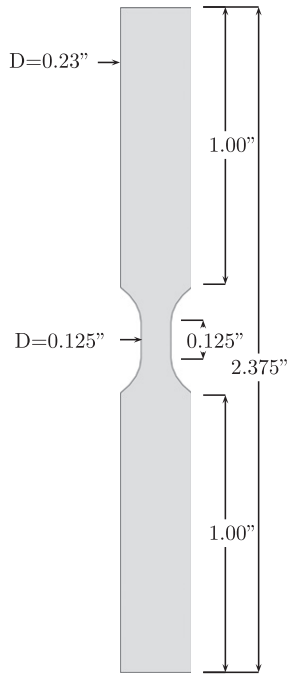

Fig. 1. Geometry and dimensions of the cylindrical specimen used in tension and compression testing.

details of the experimental procedure may be found in Littell et al. (2008).

2.3. Full-field strain measurement by digital image correlation (DIC)

A cylindrical frame of reference is associated with the specimen having $(\mathbf{e}_r, \mathbf{e}_\theta, \mathbf{e}_z)$ as base vectors. Also, a local surface frame of reference $(\mathbf{e}_1, \mathbf{e}_2, \mathbf{e}_3)$ is used with $\mathbf{e}_1 = \mathbf{e}_\theta$ in the hoop direction and $\mathbf{e}_2 = \mathbf{e}_z$ in the axial direction (Fig. 3(a)). Surface strain measurements were carried out using a non-contact digital image correlation (DIC) technique. Each tested specimen was painted with a black and white speckled pattern (Fig. 2(a)) and the displacements of the speckles were tracked during the test. The optical measurement system consists of two CCD-1330 stereo cameras (resolution down to 10^{-4} mm) and offers the possibility to measure 3D displacements. Image data processing was carried out using the DIC

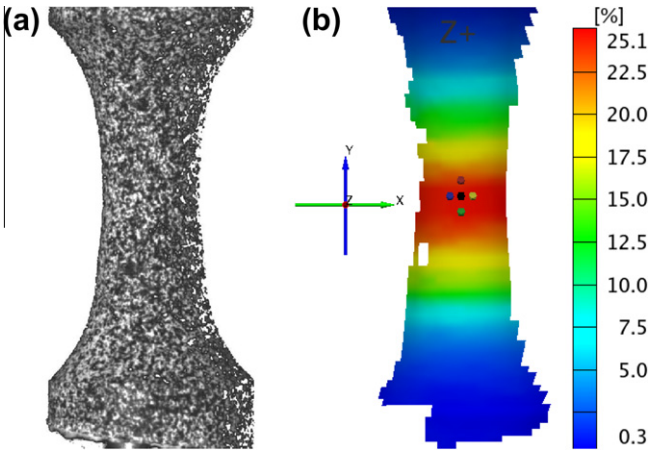

Fig. 2. (a) Gauge section of specimen painted with speckles; (b) Contours of extensional axial strain, also showing five markers used for local strain measurement.

software ARAMIS,[1] which provided the pointwise extensional and shear strains. Various choices of the local deformation tensor may be output by the software. For instance, let $\delta\mathbf{S}^{(2)} = \delta S_2 \mathbf{e}_2$ be a line element along x_2 in the reference, undeformed configuration, with x_2 being the loading axis (vertical in Fig. 2). Also, let $\delta\mathbf{s}^{(2)} = \delta s_2 \mathbf{n}$ be the deformed material element with $\mathbf{n}$. In uniaxial loading, $\mathbf{n}$ is not very different from $\mathbf{e}_2$ so long as deformation is not localized in shear bands. For the DIC software, the values of δS_2 constitute initial data and the set of values δs_2 are continuously tracked during the experiment. With that basis, one can work with the stretches $\lambda_{22} = \delta s_2/\delta S_2$, the elongations $(\delta s_2 - \delta S_2)/\delta S_2$ or the logarithmic strains $\epsilon_{22} = \ln(\lambda_{22})$. Either measure can be used in generating field maps. In what follows, we will work with the logarithmic axial strain ϵ_{22} and hoop strain ϵ_{11}. An example of full-field maps of ϵ_{22} is shown in Fig. 2b.

2.4. Video-based Surface Extensometry (VSE)

This method is based on tracking the displacement of surface markers. Two sets of markers were used for both axial and horizontal strain measurements, as sketched in Fig. 3a. The markers are also visible in Fig. 2b as large dots. The point tracking method is enabled by the DIC software. The axial and horizontal true (logarithmic) strains are defined as

$$E_{22} = \ln\left(\frac{V}{V_0}\right) \tag{1}$$

and

$$E_{11} = \ln\left(\frac{H}{H_0}\right) \tag{2}$$

where V and H respectively denote the current spacings between the vertically aligned and horizontally aligned markers (Fig. 3a), V_0 and H_0 being their initial values. The markers are located in the region where the highest strains are expected, i.e., in the central region of the gauge section. Strain uniformity between the markers was systematically studied using section line plots of DIC fields across the gauge section, as will be illustrated below.

2.5. Video-based Radial Extensometry (VRE)

One advantage of using round specimens is that when necking or barreling occur, strain gradients develop mostly in the axial direction (since no shear bands form). Because the radial strain gradients are small, measuring the diameter reduction provides a good estimate of the radial true strain. Thus, a second measure of true strain is defined based on the reduction of cross-sectional area within the neck:

$$\varepsilon = \ln\frac{S_0}{S} = 2\ln\frac{\Phi_0}{\Phi} \tag{3}$$

where S is the current cross-sectional area at the neck (or section of maximum diameter under compression), Φ is the diameter and the subscript 0 refers to initial values. If the material were incompressible, ε would be an approximation of the Hencky strain integrated over the deformation history. It is only an approximation, notably because of strain gradients in the radial direction.

Strain measure (3) requires that the diameter Φ be measured at the desired height. This measurement does not require any additional setup as it is readily accessible from camera images and the post-processing capabilities of the DIC software. More specifically, a digital tangent circle was used to fit the current deformed configuration, as sketched in Fig. 3(b). This defines a video-based

[1] ARAMIS™ GOM, Braunschweig, Germany.

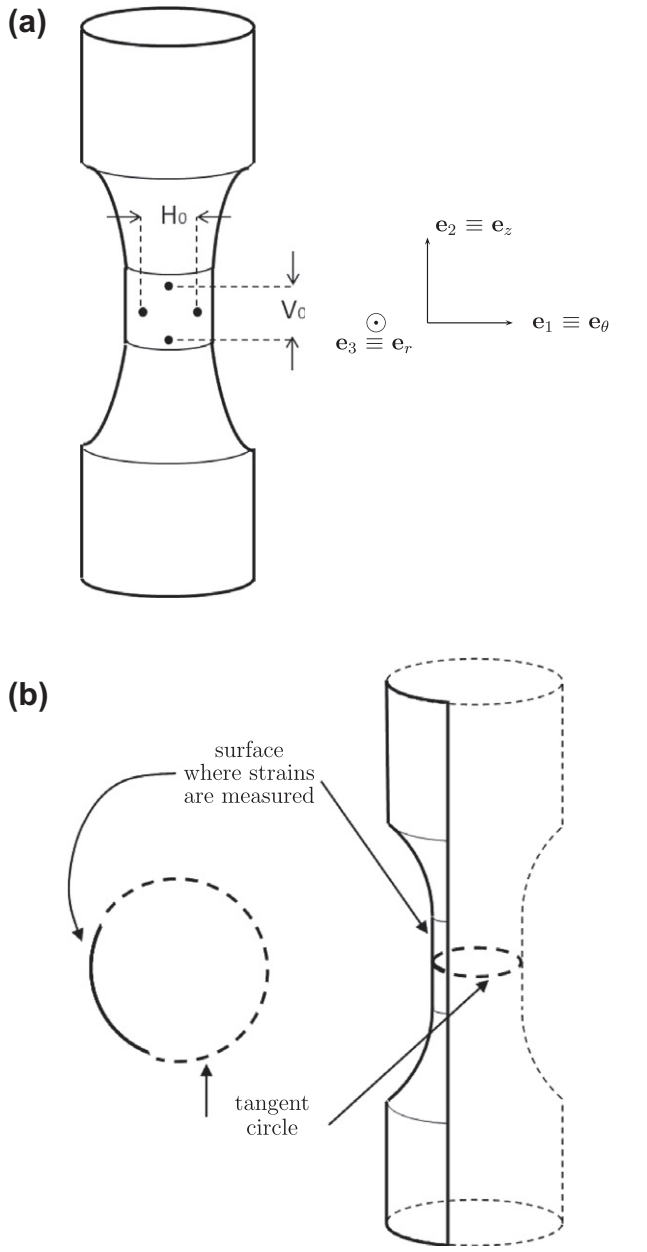

Fig. 3. (a) Video-based surface extensometry (VSE): positioning of vertical and horizontal markers. (b) Video-based radial extensometry (VRE): determination of the current cross-sectional diameter Φ in (3) and (4) using the tangent circle utility of the DIC software. Also shown in (a) is the local surface frame with associated x_1-axis (horizontal) and x_2-axis (vertical). These axes are denoted x and y in Fig. 2.

extensometer which can be implemented in real-time or after testing. 24 tension and compression tests, including those reported in Littell et al. (2008), were analyzed using this method.

2.6. True stress determination

An important consequence of video-based radial extensometry (VRE) is that the true stress can be evaluated as

$$\sigma^{\mathrm{VRE}} \equiv \sigma = \frac{F}{S} = \frac{4F}{\pi\Phi^2} \tag{4}$$

where both F (the force given by the load cell) and Φ (the diameter) are measured. Thus, curves of the above measure of true stress, σ, versus the true strain measure ε in (3) constitute the output of VRE.

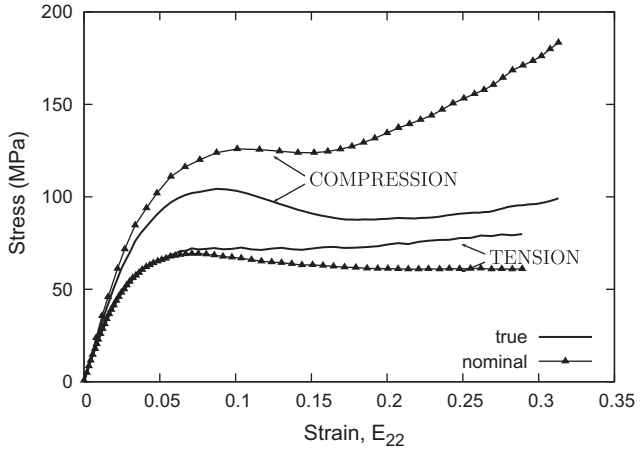

Fig. 4. Comparison between the nominal stress σ^{eng} and the true stress σ in (4) both as a function of E_{22} in (1). Example 1: compression at $\dot{\epsilon} = 10^{-1}$/s; Example 2: tension at $\dot{\epsilon} = 10^{-5}$/s.

On the other hand, when using surface markers (VSE) or DIC strains further assumptions must be used to calculate the stress. An estimate of the true stress associated with the VSE true strain measure E_{22} in (1), assuming that is the only available strain measure, is given by

$$\sigma^{\mathrm{VSE;2}} = \frac{F}{S_0}\exp(E_{22}). \tag{5}$$

where material incompressibility[2] and isotropy[3] are assumed. Note that the remote uniaxial stress state is assumed to hold on the surface between the vertically aligned markers. Similarly, the following true stress is associated with the VSE horizontal strain E_{11} in (2)

$$\sigma^{\mathrm{VSE;1}} = \frac{F}{S_0}\exp(-2E_{11}) \tag{6}$$

since $S = S_0\lambda_{rr}^2$ where the radial stretch λ_{rr} is identified with $\lambda_{\theta\theta} = \lambda_{11}$. Eq. (6) relaxes the assumption of incompressibility. If there are no axial strain gradients $\sigma^{\mathrm{VSE;1}} \approx \sigma^{\mathrm{VSE;2}}$ to the neglect of elastic compressibility.

Likewise, an estimate of the true stress associated with the DIC true strain measure ϵ_{22}, assuming that is the only strain measure available, is given by

$$\sigma^{\mathrm{DIC}} = \frac{F}{S_0}\exp(\epsilon_{22}).$$

where material incompressibility and isotropy are assumed as above. Note that the remote uniaxial stress state is assumed to hold locally on the surface. A better estimate of the true stress is obtained by using the DIC hoop strain ϵ_{11} using

$$\sigma^{\mathrm{DIC}} = \frac{F}{S_0}\exp(-2\epsilon_{11})$$

which relaxes the assumption of incompressibility. In principle, if not in practice, the local true stress–strain response may then be estimated using σ^{DIC} from either equation above versus ϵ_{22}. However, we shall not pursue this option because, even in the presence of rather weak instabilities, the location of the maximum strain within the gauge section changes during loading.

[2] Plastic incompressibility is obeyed in many glassy polymers. The material is compressible in the elastic regime.

[3] It is indeed checked *a posteriori* that initially round sections remain round after deformation.

3. Results

3.1. Nominal stress–strain response

For illustration, curves of the nominal stress $\sigma^{\text{eng}} \equiv F/S_0$ versus axial strain E_{22} given by (1) are shown in Fig. 4. One example is for compression at $\dot{\epsilon} = 10^{-1}/\text{s}$; the other is for tension at $\dot{\epsilon} = 10^{-5}/\text{s}$. In each case, the nominal stress is compared with the true stress σ given by (4). While obvious differences are expected at large strains, Fig. 4 clearly shows that the engineering stress deviates from the true stress more significantly in compression than it does in tension. For example, at the peak stress in compression the difference between the two measures is a little over 20 MPa and increases to about 80 MPa at larger strains. In tension, the difference is smaller; as will be illustrated below, this is due to the fact that barreling in compression is more pronounced than is necking in tension. One reason for the absence of strong localization under tension is the cylindrical geometry and the length of the gauge section, which is quite short thus preventing significant neck propagation from occurring.

3.2. Video surface versus radial extensometry

We now proceed to compare the true stress–strain responses obtained using VSE (surface markers) and video-based radial extensometry (VRE). VSE employs stress measure (5) versus axial strain measure E_{22} in (1) whereas VRE uses σ in (4) versus ε in (3). Comparison is illustrated in Fig. 5 for a typical case in tension. The two responses are very close to each other with the VSE based stress measure (5) leading to a slightly harder response. As shown in Fig. 5(b), the strain measures ε (diameter based) and E_{22} (markers based) are also very close to each other. The maximum relative difference between the two was less than 15% with a 5% difference being typical. For our purposes, the measures ε and E_{22} will be considered as indistinguishable in tension.

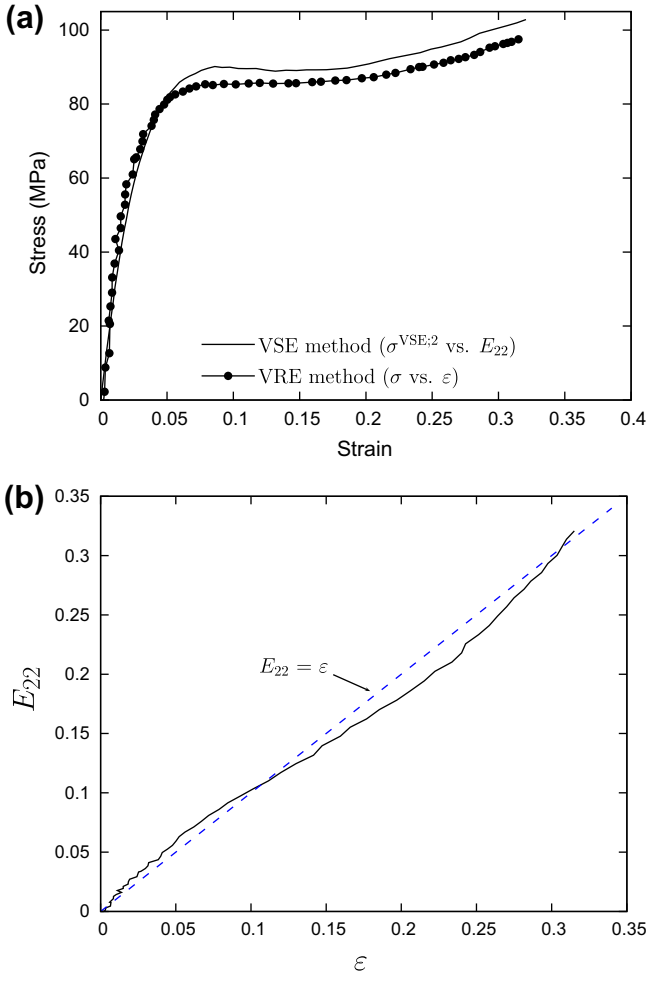

Fig. 5. (a) True stress–strain curves in tension obtained using video-based extensometry (VSE vs. VRE). (b) Video based surface extensometry (axial) strain measure E_{22} in (1) versus video-extensometer based ε in (3). Here, $\dot{\epsilon} = 10^{-3}/\text{s}$.

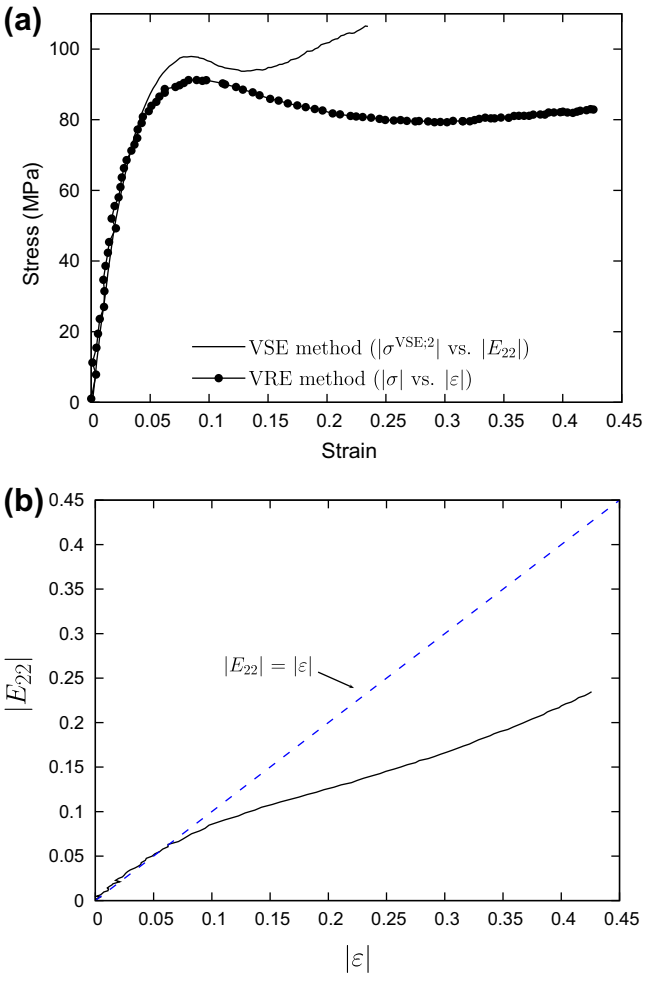

Fig. 6. (a) True stress–strain curves in compression obtained using video-based extensometry (VSE vs. VRE). (b) Video based surface extensometry (axial) strain measure E_{22} in (1) versus video-extensometer based ε in (3). Here $\dot{\epsilon} = 10^{-3}/\text{s}$.

In compression, however, the situation is different as typically shown in Fig. 6. The flow strength levels are found to be increasingly higher with the VSE based stress measure (5) compared with the VRE based measure (4). As shown in Fig. 6(b), the main discrepancy between the two methods resides in the strain determination. The VSE strain measure E_{22} is found to be considerably smaller than the VRE measure ε in the plastic regime. This difference occurs subsequent to necking-induced strain localization. Despite the fact that E_{22} has more of a local character, it was systematically found to be smaller than the diameter-based measure ε, irrespective of strain rate or whether the testing was in tension or compression.[4]

[4] There is only one exception among all experiments: one case of tension at $\dot{\epsilon} = 10^{-3}/\text{s}$ shows end-of-test values of $\varepsilon = 0.32$ and $E_{22} = 0.38$. The corresponding realization is shown in Fig. 8.

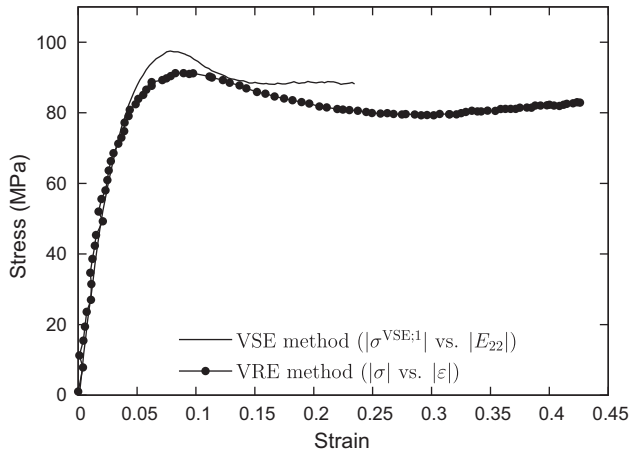

Fig. 7. True stress–strain curves in compression obtained using video-based surface extensometry as customary in the literature versus VRE.

For reference, published VSE based works (G'Sell et al., 2002; Gloaguen and Lefebvre, 2001; Mohanraj et al., 2006) have exclusively used the axial strain E_{22} in generating true stress–strain curves. It is noteworthy that these authors used stress definition (6) instead of (5). This is always better since (6) does not assume incompressibility. However, the assumption of incompressibility is not relevant here. To verify this, Fig. 7 depicts the comparison between the VSE stress–strain curve as obtained in the above works and the VRE σ-ε curve. Important differences remain. In the presence of strong localization, as is the case in compression here, these differences are associated with a problem in using the axial strain measure E_{22} when there are axial strain gradients. This issue is now addressed through detailed comparisons with DIC strain fields.

3.3. DIC based assessment of VBE methods

An important difference between E_{22} and ε is that the former is a surface measurement whereas the latter smears out the radial strain gradients in the specimen. However, the large discrepancies found in compression between the two measures cannot be explained on that basis. In order to appreciate these differences further, it is worth examining the phenomenology of deformation in EPON 862 by correlating the full-field strain mapping with video-based strain measures and the overall stress–strain response.

Fig. 8 illustrates such a correlation in the case of tension (the test realization being different from that in Fig. 5). The contours of axial strain are shown using the same scale. Prior to the peak yield, the polymer behavior is nonlinear. At a strain of $E_{22} = 0.083$, i.e., slightly before peak, the strain distribution is essentially homogeneous within the gauge area, Snapshot (A). Shortly thereafter, deformation localizes because of the development of a shallow neck. Difficult to visualize with the naked eye, the onset of necking is ascertained based on two observations: (i) the drop in the force, as seen for example in the nominal curve of Fig. 4; and (ii) the deformation becomes nonuniform along the x_2-axis (Snapshot (B) in Fig. 8). In actuality, localization is likely to have set in earlier than stage (B). This can be ascertained based on the line section plots in Fig. 8(b). For each value of VSE strain E_{22} the corresponding DIC strain ϵ_{22} is plotted along the vertical line shown in the inset. Local strains reach values around 0.20 and decrease down to about 0.08 near the ends of the specimen gauge section. Subsequent deformation is characterized by a rehardening regime starting at a strain of about $E_{22} = 0.14$. As a consequence, material in the vicinity of the incipient neck hardens again and deformation becomes more diffuse going from snapshot (B) to (D) through (C). Finally, fracture takes place at a strain of about $E_{22} = 0.39$. The corresponding snapshot (D), taken right before fracture, exhibits some strain concentration at the center with most of the gauge section experiencing strains higher than 0.3.

The asymmetry of the DIC strain profiles in Fig. 8(b) implies that neck initiation occurs at a random location. The shift of the location of the maximum strain is the signature of neck propagation. Each strain profile is indexed with the marker-based VSE strain E_{22}. There is a very good correspondence between the maximum local strain ϵ_{22}^{max} and E_{22}, hence between ϵ_{22}^{max} and the VRE measure ε, given the results in Fig. 5.

Fig. 9 depicts a typical response in uniaxial compression as well as snapshots of strain contours at various stages of deformation. As

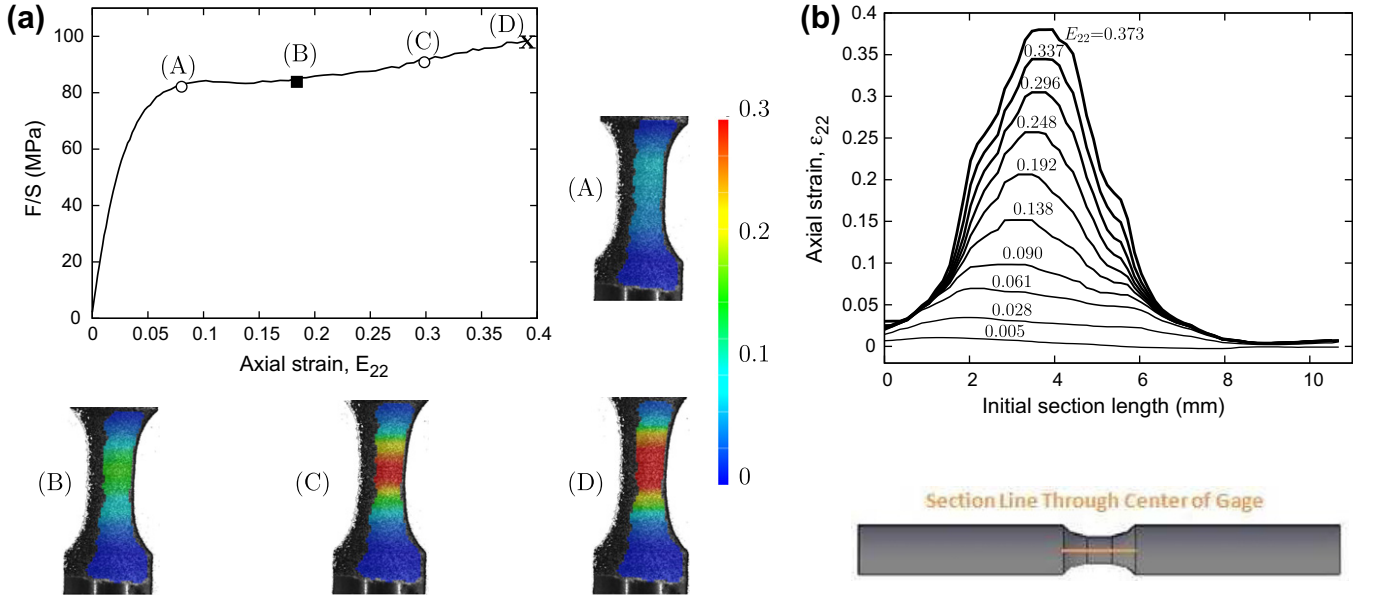

Fig. 8. (a) True stress σ versus true strain E_{22} and corresponding select snapshots of DIC strain contours in tension at $T = 25$ °C and $\dot{\epsilon} = 10^{-3}$/s. (b) Section line plots of axial strain ϵ_{22} at various levels of logarithmic axial strain E_{22}, showing the progress of localization. The circles on the curve in (a) correspond to stages before and after the onset of necking (resp. (A) and (C)), which is observable at (B). The cross indicates fracture which occurs slightly after stage (D).

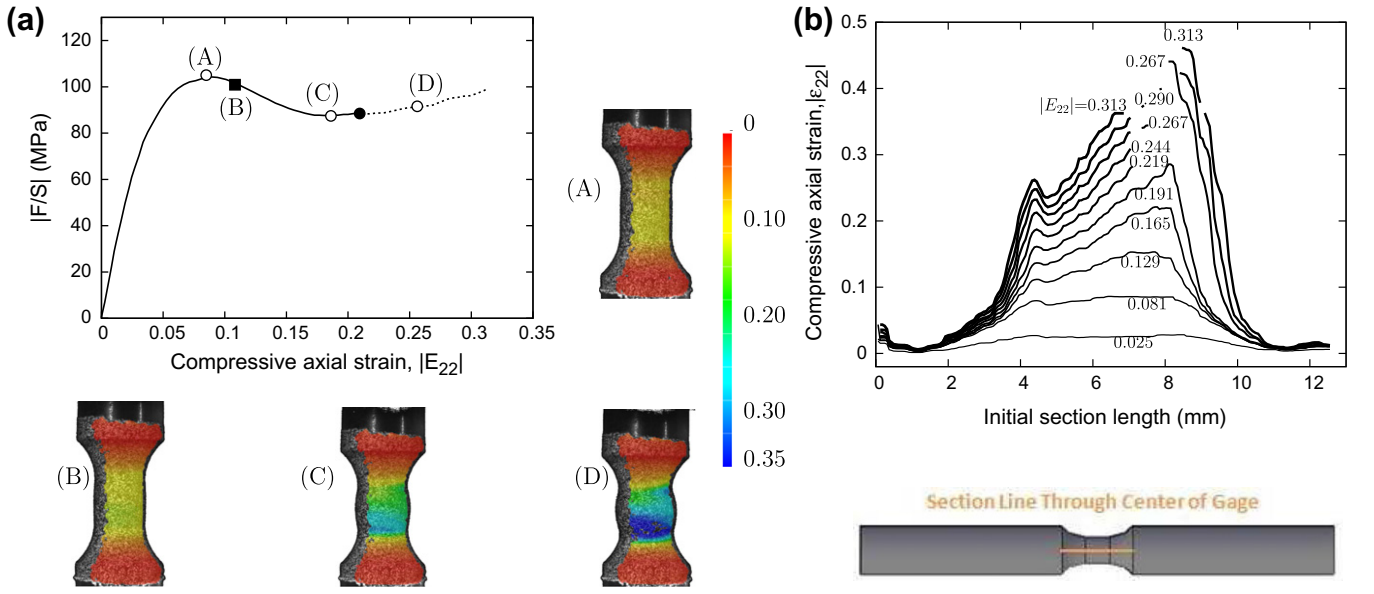

Fig. 9. (a) True stress σ versus true strain E_{22} and corresponding select snapshots of DIC strain contours in compression at $T = 25$ °C and $\dot{\epsilon} = 10^{-1}$/s. (b) Section line plots of axial strain ϵ_{22} at various levels of logarithmic strain E_{22}, showing the progress of localization. The circles on the curve in (a) correspond to stages before and after the onset of barreling (resp. (A) and (C)), which is clearly observable at (B). The full circle indicates the loss of consistency of DIC data.

observed in tension, the strains at peak stress ($\sigma = 102$ MPa) are rather homogeneous (snapshot A). During the softening regime, barreling becomes clear within the specimen gauge (snapshot B). Additional compression is accompanied by a growing barreling instability as well as strain concentrations. The lower yield stress ($\sigma = 87$ MPa), is reached at E_{22}= 0.18. A mapping of strains at the beginning of the rehardening stage is detailed in snapshot (C). Contrary to tension, a more asymmetric strain distribution pattern develops in the specimen. In this particular case, the maximum compressive strains are obtained in the lower half of the gauge section. It is likely that the asymmetry in strain distribution is caused by the non-standard specimen geometry. The strain profiles in Fig. 9(b) quantify the strong localization of plastic flow under compression.

Going back to the difference between the two strain measures E_{22} in (1) and ε in (3) (see Fig. 6), the picture is now much clearer in light of the results shown in Figs. 8 and 9. In particular, barreling in compression often leads to a strain distribution that is asymmetric with respect to the horizontal x_1-axis. Because the strain measure E_{22} includes some material points above and below the section of maximum diameter, its value is smaller than the maximum strain. In tension, local strain variations are smaller between the vertical markers. Note that in longer specimens this may not hold true. In some cases, the two measures lead to nearly identical stress–strain curves (e.g. Fig. 5(a), 10^{-3}/s), but in other cases (e.g. at 10^{-5}/s), some differences are noted, although less dramatic than under compression loading.

To complete the picture, Fig. 10 shows the same local strain profiles as in Fig. 9(b) but now indexed with the diameter-based VRE strain measure ε. Not only is there good correspondence in the early stages of deformation between $\epsilon_{22}^{\max}$ and ε, the latter takes larger values at the later stages of deformation. This might seem surprising at first sight but can be explained by the development of a complex stress state on the surface of a barreled specimen. Indeed, analysis indicates that tensile hoop stresses develop on the surface (Kweon and Benzerga, in press-a) which lead to axial surface strains that are smaller in magnitude than at the center of the specimen. It is believed that the value of $\varepsilon = 0.539$ is close to the value at the center of the bar. In any case, differences between ε and $\epsilon_{22}^{\max}$ remain rather small and the above comparisons (i) validate video-based *radial* extensometry (VRE); and (ii) show that a strain measure based on vertically aligned markers is not reliable.

The DIC software may not be capable of capturing and calculating strains in highly deformed regions (dark spots in Fig. 9 at stage (D)). When such problems occur in the center of the specimen, where strain values are used for post-processing the measure E_{22}, the software calculates the strain at a nearby location, which is problematic for consistency. In the example shown, this data capturing problem occurred at a strain of about $E_{22} = 0.215$. It is indicated by a filled circle in the figure. The data acquired beyond this point is plotted as a dotted line, simply to indicate that it may not be as reliable as data before that stage. Snapshot (D) depicts the strain contours at E_{22}= 0.255. The strain distribution is heterogeneous with maxima exceeding a value of 0.35, concentrated at the bottom of the gauge section.

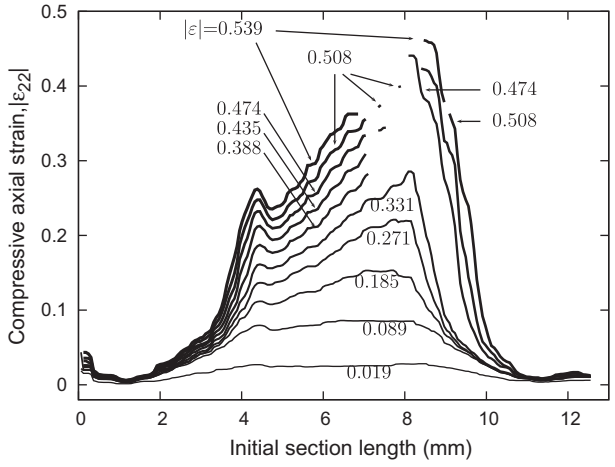

Fig. 10. Profiles of DIC axial strain ϵ_{22} corresponding to increasing values of the VRE strain ε.

3.4. VSE with horizontal markers

When comparing the stress–strain responses in Figs. 6(a) and 7 the discrepancy between flow stress levels in the latter is much

smaller than in the former. The difference is that the horizontal-marker based strain measure E_{11} is used in calculating the stress plotted in Fig. 7, as per Eq. (6). In the compression specimen, strain gradients develop post-barrelling mostly in the axial direction of the specimen thus affecting strongly the strain measure E_{22}. On the other hand, the strain gradients are smaller in the x_1 direction (Fig. 9(b)) so that the transverse measure E_{11} is less affected by strain localization.

In what follows, we therefore describe results obtained using a variant of the VSE method for determining the true stress–strain response whereby $|2E_{11}|$ is used instead of $|E_{22}|$ as an estimate of axial true strain, assuming incompressibility. Typical stress–strain curves obtained with this method are compared with those obtained using the VRE method (Eqs. (4) and (3)) in Figs. 11(a) and (b). What is interesting is that the two curves are close to each other, both under tension and compression. Fig. 11(c) shows how $|\varepsilon|$ and $2|E_{11}|$ evolve against each other for both tests considered. The two strain measures take identical values before the onset of plastic instability. Subsequent to that, measure ε is found to be greater. The difference between the two measures increases at first with straining but eventually decreases such that at a strain of about 0.4 the two measures are almost identical. Analysis (Kweon and Benzerga, 2013) indicates that the strain is maximum at the center of the bar but $2E_{11}$ is based on a surface measure. In addition, since the horizontal markers are positioned prior to testing, the location of the maximum of $2E_{11}$ may be away from the exact location of the neck (in tension) or barrel's apex (in compression). With such limitations in mind and with appropriate care, it may be convenient in general to work with true stress–strain curves obtained using this variant of the VSE based procedure instead of the commonly used one based on vertically aligned markers.

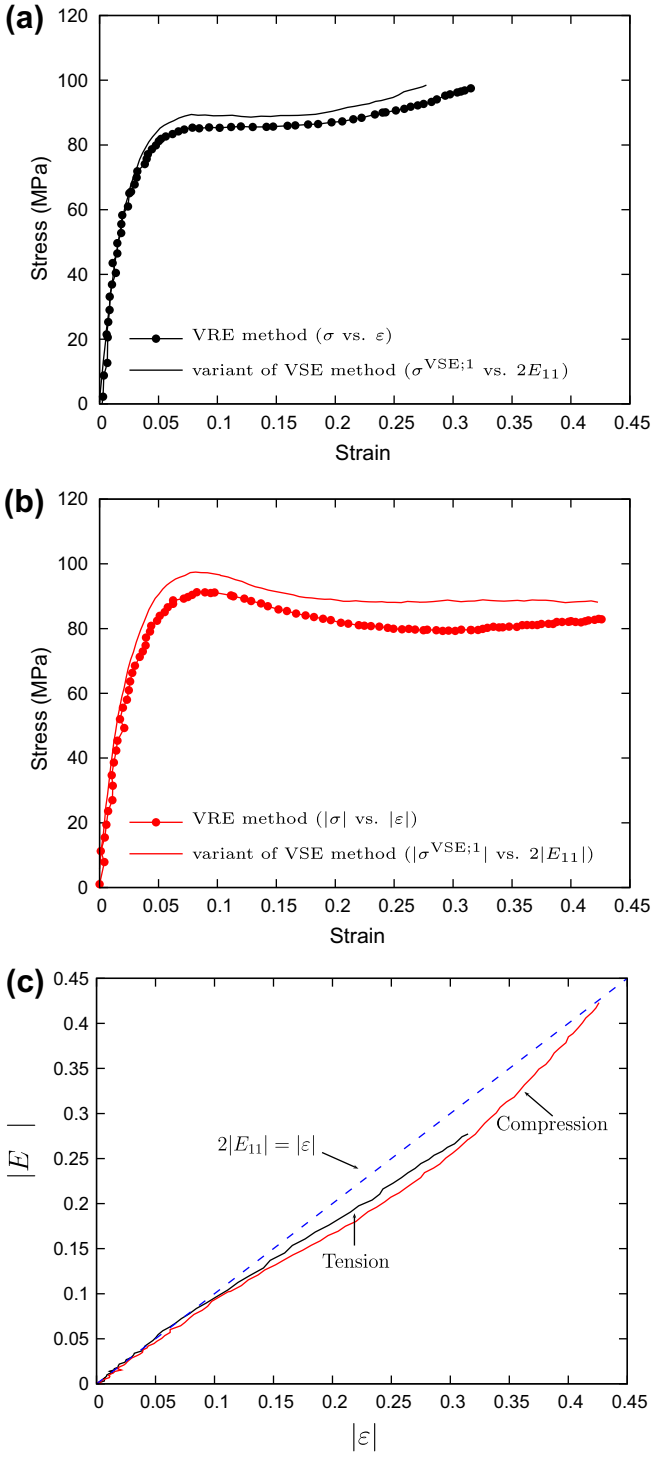

Fig. 11. True stress–strain responses of epon 862 to (a) tension and (b) compression at $T = 25$ °C and $\dot{\epsilon} = 10^{-3}$/s. (c) Strain measure $2|E_{11}|$ in (2) versus $|\varepsilon|$ for both tests.

4. Discussion

The fundamental hypothesis in identifying the mechanical response of a specimen with the intrinsic behavior of the constituent material is that the deformation is homogeneous within the specimen gauge. When deformation ceases to be uniform, the response is inherent to the specimen, not to the material. The tacit question addressed in this experimental study is therefore that of what *practical* measures of true stress and true strain, if any, would deliver the best approximation of the *exact* true stress–strain relation. This involves identifying a representative elementary volume, within the test specimen, over which nonuniformities are weak enough to allow for the sought identification.

Over the past decade, experiments aimed at extracting the intrinsic behavior of polymeric materials from tensile tests have employed either whole field strain measurements or video extensometry with some variations. In this study, the different approaches have been compared. In all previous work based on the marker tracking variant of video extensometry, the true stress was determined by calculation assuming that deformation is homogeneous between vertically or horizontally aligned markers. Here, a version of video extensometry compatible with the DIC set-up was used to obtain the true stress by direct measurement of the instantaneous diameter of the minimum cross-section at the evolving neck. While this measurement provides a net normal stress, it is preferred to the local estimation of the true stress, as for example done by Gloaguen and Lefebvre (2001). This is so because when strong strain localization sets in, the local stress–strain behavior is generally affected by neck progression as inferred, for example, from finite-element analyses of structural instabilities in glassy polymers (Kweon and Benzerga, 2013); see also Parsons et al. (2004).

Digital image correlation (DIC) is a powerful mapping technique that provides more information than the minimum necessary for material behavior identification. In the case of the investigated epoxy resin, the DIC measurements allowed a critical assessment of video-based extensometry. We have shown that the stress–strain responses based on both techniques (VSE and VRE) are quite close to each other in the absence of strong (specimen-level) localization. However, the case of compression (Fig. 6) shows that one cannot entirely rely on VSE based data when strong localizations occur. Measures such as E_{22} are inevitably impacted by the effects of the structural instability. In that case, the VRE method delivers a much more accurate determination of stress–strain behavior.

The differences seen here between tension and compression should not be mistakenly generalized. In general, strong localizations are indeed more likely under tension loading because of neck propagation or shear-band mediated necking. Some factors that have limited the extent of tensile localization in this study include (i) the material used; (ii) the short length of the gauge section and (iii) the use of round specimens as opposed to prismatic rectangular ones where shear bands are usually observed.

Any attempt at inferring the true stress from the nominal one using an axial strain measure will suffer some artifacts. The approximate stress measure (6), i.e., estimated based on horizontal markers, provides an alternative way of calculating the true stress. This method may be attractive when video radial extensometry is not available. As shown in Fig. 11, the stress–strain curves inferred from this method are very close to the σ-ε curves. However, such good correspondence may break down under circumstances of strong strain localization, i.e., with lateral strain gradients in rectangular specimens.

Determination of the intrinsic behavior of polymers is essential before making inferences about salient features of their constitutive response and the underlying physics of deformation mechanisms. Some features of the intrinsic response of Epon 862 are worth discussing. As shown in Fig. 4 this epoxy is able to sustain very large strains, even in tension. To our knowledge, the tensile ductility levels revealed by the present measurements are unprecedented for an epoxy resin. In the literature, tension data is often reported up to a few percents of total strain because of premature fracture. Together with results from previous investigations (Goldberg et al., 2005) the present results clearly show that this behavior is an artifact of using strain gauges. The latter concentrate strains and thus lead to specimen failure. More generally, fracture is affected by processing-induced internal voids (Chowdhury et al., 2008b), surface flaws and stoichiometry variations. In this work, the density of voids was minimized by using precision tooling and a pressurized RTM process to fabricate the panels. Major surface flaws were avoided by using a cylindrical specimen shape (no corners), CNC machining and non-contact strain measurement. For the commercial Epon 862 that has been used, systematic characterizations of different resin systems were carried out at NASA. Reporting on these goes beyond the scope of this paper. What is of particular importance, however, is that standard (hence larger) specimens with rectangular cross-section, with mounted extensometers or glued strain gauges, failed at much lower strains than the small, cylindrical test specimens.

There also is a connection between tensile ductility and post-yield softening, as pointed out by van Melick et al. (2003a). In the studied Epon 862, the strain softening is very small in tension. This is not the case of other previously investigated materials, e.g. (Liang and Liechti, 1996). It is likely that the higher amount of softening, which may be due to different processing histories, is responsible for the lower ductility levels reported by previous studies.

In tension, the true stress–strain curve is characterized by a hardening stage at small strains, followed by a plateau then a rehardening stage at larger strains. It is likely that the true tensile behavior exhibits a weak post-yield strain softening, given that the net stress measure σ slightly overestimates the actual true stress (Kweon and Benzerga, 2013). In compression, the amount of post-peak softening is noticeable. The care taken in analyzing the data leads us to conclude that this softening is intrinsic to the material behavior. The magnitude of the difference between tension softening and compression softening post-yield is likely to be smaller than reported here. Nevertheless, it is a finding based on consistent and repeatable experimental measurements. This difference may be associated with the microscopic processes of free-volume rearrangement in the early stages of shear yielding and how such processes are affected by the amount of hydrostatic pressure or, more generally, by some stress-state dependence. This aspect of tension–compression asymmetry has not been discussed in the literature, probably because of the scarcity of data available in both tension and compression for the same polymer.

The VRE strain measure ε has some limitations as well. For example, the stress–strain data is not reliable in the elastic regime because of the underlying assumption of material incompressibility. Next, some challenges arise in measuring the diameter with sufficient accuracy in the early stages of deformation. For instance, some serrations can be clearly see in Fig. 5(a). However, both limitations hold for the small strain regime, during which deformation is homogeneous. Thus, they do not affect the central issues of the study, i.e., the intrinsic character of any post-yield softening and the large-strain behavior.

It is worth examining how the above differences among the various methods impact the identification of the polymer behavior and that of material parameters in advanced polymer models, e.g. (Arruda et al., 1995; Wu and Van, 1993; Chowdhury et al., 2008a; Klompen et al., 2005). The key in understanding is to decouple the unavoidable structural effects from the intrinsic behavior. Here, we distinguish two cases: one where strain gradients are mostly axial (as is favored in round specimens) and one where strain gradients occur both axially and radially, as is expected in rectangular (thin or thick) specimens. The latter have been extensively reported in the literature and often lead to the formation of propagating shear bands. If the evolving localization is such that strain gradients are mostly in the axial (loading) direction then the best material–structural decoupling is ensured by using video-based extensometry (the σ-ε curves). In the second case, the shear-band mediated propagation of tensile necks creates challenges for all measures. However, if the post-yield drop is moderate, analysis indicates that the σ-ε curves provide again an accurate representation of intrinsic behavior (Kweon et al., submitted for publication). Some authors have proposed the use of inverse identification to extract the intrinsic behavior, using full boundary-value problem solutions. While, in principle, this is possible, in practice it proves challenging because the local stress–strain response is itself affected by the onset and propagation of instabilities.

5. Conclusion

Whole-field strain measurements were obtained in combination with video-based radial extensometry and marker tracking to study the inhomogeneous deformation of a polymer. An experimental methodology was proposed to extract the intrinsic behavior of polymers from the mechanical response of tensile and compression specimens. The method is applicable in the presence of moderate structural instabilities. The main conclusions of this study are:

- Video-based extensometry delivers approximately work-conjugate measures of true stress and strain. The corresponding stress–strain curve represents the large strain intrinsic behavior of the material fairly well, as validated by comparison with DIC based measurements. Any disadvantages due to the assumption of incompressibility or the inaccuracy of curvature measurement manifest exclusively at small strains when the specimens deform homogeneously.
- Care should be taken in using strain measures based on vertically aligned markers, a common technique of video extensometry. They may not represent the true strain well in the presence of moderate to strong strain localization.
- In tension, the true stress–strain curve of Epon 862 is characterized by a hardening stage at small strains, followed by a plateau then a rehardening stage at larger strains. The amount of

softening, if any, is very small. In compression, the amount of post-peak softening is noticeable. This aspect of tension–compression asymmetry indicates a strong dependence of the yield process on the stress state.

Acknowledgement

The authors acknowledge support from NASA Glenn Research Center under cooperative agreement NNX07AV39A between Texas Engineering Experiment Station and GRC, and cooperative agreement NNX07AV60A between the University of Akron and GRC. The authors would also like to thank Tim Woodburry from TAMU for his assistance with video-monitored post-processing of test results.

References

Arruda, E.M., Boyce, M.C., Jayachandran, R., 1995. Effects of strain rate, temperature and thermomechanical coupling on the finite strain deformation of glassy polymers. Mech. Mater. 19, 193–212.

ASTM, 2008. D638-08: standard test method for tensile properties of plastics. ASTM International.

Benzerga, A.A., Besson, J., Pineau, A., 2004. Anisotropic ductile fracture. Part I: Experiments. Acta Mater. 52, 4623–4638.

Beremin, F.M., 1981. Experimental and numerical study of the different stages in ductile rupture: application to crack initiation and stable crack growth. In: Nemat-Nasser, S. (Ed.), Three-Dimensional Constitutive relations of Damage and Fracture. Pergamon Press, North Holland, pp. 157–172.

Bowden, P.B., Jukes, J.A., 1968. The plastic yield behaviour of polymethylmethacrylate. J. Mater. Sci. 3, 183–190.

Boyce, M.C., Arruda, E.M., 1990. An experimental and analytical investigation of the large strain compressive and tensile response of glassy polymers. Polym. Eng. Sci. 30, 1288–1298.

Buisson, G., Ravi-Chandar, K., 1990. On the constitutive behavior of polycarbonate under large deformation. Polymer 31, 2071–2076.

Chowdhury, K.A., Benzerga, A.A., Talreja, R., 2008a. A computational framework for analyzing the dynamic response of glassy polymers. Comput. Methods Appl. Mech. Eng. 197, 4485–4502.

Chowdhury, K.A., Talreja, R., Benzerga, A.A., 2008b. Effects of manufacturing-induced voids on local failure in polymer-based composites. J. Eng. Mat. Tech. 130, 021010.

Fang, Q.-Z., Wang, T.J., Beom, H.G., Zhao, H.P., 2009. Rate-dependent large deformation behavior of pc/abs. Polymer 50, 296–304.

Gilat, A., Goldberg, R.K., Roberts, G.D., 2007. Strain rate sensitivity of epoxy resin in tensile and shear loading. J. Aerospace Eng. 20, 75–89.

Gloaguen, J.M., Lefebvre, J.M., 2001. Plastic deformation behavior of thermoplastic/clay nanocomposites. Polymer 42, 5841–5847.

Goldberg, R.K., Roberts, G.D., Gilat, A., 2005. Implementation of an associative flow rule including hydrostatic stress effects into the high strain rate deformation analysis of polymer matrix composites. J. Aerospace Eng. 18, 18–27.

Grytten, F., Daiyan, H., Polanco-Loria, M., Dumoulin, S., 2009. Use of digital image correlation to measure large-strain tensile properties of ductile thermoplastics. Polymer Test. 28, 653–660.

G'Sell, C., Gopez, A.J., 1981. Plastic banding in glassy polycarbonate under plane simple shear. J. Mater. Sci. 20, 3462–3478.

G'Sell, C., Jonas, J.J., 1979. Determination of the plastic behavior of solid polymers at constant true strain rate. J. Mater. Sci. 14, 583–591.

G'Sell, C., Hiver, J.M., Dahoun, A., Souahi, A., 1992. Video-controlled tensile testing of polymers and metals beyond the necking point. J. Mater. Sci. 27, 5031–5039.

G'Sell, C., Hiver, J.M., Dahoun, A., 2002. Experimental characterization of deformation damage in solid polymers under tension, and its interrelation with necking. Int. J. Solids Struct. 39, 3857–3872.

Hasan, O.A., Boyce, M.C., Li, X.S., Berko, S., 1993. Investigation of the yield and postyield behavior and corresponding structure of poly(methyl methacrylate). J. Polymer Sci. Part B Polymer Phys. 31 (2), 185–197.

Haward, R.N., Thackray, G., 1968. The use of a mathematical model to describe isothermal stress–strain curves in glassy thermoplastics. Proc. Roy. Soc 302, 453.

Hild, F., Roux, S., 2006. Digital image correlation: from displacement measurement to identification of elastic properties – a review. Strain 42, 69–80.

Klompen, E.T.J., Engels, T.A.P., Govaert, L.E., Meijer, H.E.H., 2005. Modeling of the postyield response of glassy polymers: influence of thermomechanical history. Macromolecules 38, 6997–7008.

Kweon, S., Benzerga, A.A., in press-a. Finite element implementation of a macromolecular viscoplastic polymer model. Int. J. Numer. Methods Eng.

Kweon, S., Benzerga, A.A., 2013. On the localization of plastic flow in glassy polymers. Eur. J. Mech. 39, 251–267.

Kweon, S., Poulain, X., Benzerga, A.A., submitted for publication. On the intrinsic behavior of polymers in tension.

Laraba-Abbes, F., Ienny, P., Piques, R., 2003. A new 'tailor-made' methodology for the mechanical behavior analysis of rubber-like materials: I. Kinematics measurements using a digital speckle extensometry. Polymer 44, 807–820.

Liang, Y.-M., Liechti, K.M., 1996. On the large deformation and localization behavior of an epoxy resin under multiaxial stress states. Int. J. Solids Struct. 33, 1479–1500.

Littell, J.D., Ruggeri, C.R., Goldberg, R.G., Roberts, G.R., Arnold, W.A., Binienda, W.K., 2008. Measurement of epoxy resin tension, compression, and shear stress–strain curves over a wide range of strain rates using small test specimens. J. Aerospace Eng. 21, 162–173.

Ma, Z., Ravi-Chandar, K., 2000. Confined compression: a stable homogeneous deformation for constitutive characterization. Exp. Mech. 40, 38–45.

Mohanraj, J., Barton, D.C., Ward, I.M., Dahoun, A., Hiver, J.M., G'Sell, C., 2006. Plastic deformation and damage of polyoxymethylene in the large strain range at elevated temperatures. Polymer 47, 5852–5861.

Parsons, E., Boyce, M.C., Parks, D.M., 2004. An experimental investigation of the large-strain tensile behavior of neat and rubber-toughened polycarbonate. Polymer 45, 2665–2684.

Ravi-Chandar, K., Ma, Z., 2000. Inelastic deformation in polymers under multiaxial compression. Mech. Time-Dependent Mater. 4, 333–357.

Santore, M.M., Duran, R.S., McKenna, G.B., 1991. Volume recovery in epoxy glasses subjected to torsional deformations: the question of rejuvenation. Polymer 32, 2377–2381.

Shield, T.W., Kim, K.S., 1991. Diffraction theory of optical interference moire and a device for production of variable cirtual reference gratings. a moire microscope. Exp. Mech. 31, 126–134.

Tack, J.L., Ford, D.M., 2008. Thermodynamic and mechanical properties of epoxy resin DGEBF crosslinked with DETDA by molecular dynamics. J. Molecular Graph. Model. 26, 1269–1275.

van Melick, H.G.H., Govaert, L.E., Meijer, H.E.H., 2003a. Localisation phenomena in glassy polymers: influence of thermal and mechanical history. Polymer 44, 3579–3591.

van Melick, H.G.H., Govaert, L.E., Meijer, H.E.H., 2003b. On the origin of strain hardening in glassy polymers. Polymer 44, 2493–2502.

Wu, J.J., Buckley, C.P., 2004. Plastic deformation of glassy polystyrene: a unified model of yield and the role of chain length. J. Polymer Sci. 42, 2027–2040.

Wu, P.D., Van der Giessen, E., 1993. On improved network models for rubber elasticity and their applications to orientation hardening in glassy polymers. J. Mech. Phys. Solids 41, 427–456.